7 CHAPTER

SEGMENTATION OF MRI DATA USING MULTI-OBJECTIVE ANTLION BASED IMPROVED FUZZY C-MEANS

Highlights of the Chapter

- *The robust segmentation of magnetic resonance imaging (MRI) data relies on multi-objective antlion optimization approach for Fuzzy c-mean algorithm*
- *An approach to find the optimal number of clusters presents in the image produced notable results*
- *The algorithm has been tested and validated on a 62 dataset of images contains synthetic images and simulated MRI images*

Abstract

The present work proposes the robust segmentation of magnetic resonance imaging (MRI) data relies on multi-objective approach in the Fuzzy c-mean algorithm. The fitness functions cluster compactness and fuzzy hyper-volume calculated over the local spatial and gray scale information of the image. Multi-objective antlion optimization minimizes these fitness functions and produces the non-dominating set of solutions called Pareto fronts. Further, fuzzy clustering measure Partition entropy coefficient helps to select most promising

segmentation from Pareto fronts to achieve the optimum segmentation. In addition to this, present work also proposes a new approach to find the optimal number of clusters presents in the image. The proposed algorithms are extensively tested on thirty-two synthetic images corrupted with Gaussian and speckle noises with different noise levels and thirty simulated brain MRI data. The results were compared with existing similar methods, where the proposed algorithms demonstrate the superior performance in terms of accuracy.

7.1 Introduction

The computer-aided diagnosis assists radiologists to interpret the information contains in the image, where the accuracy of diagnosis highly depends on the segmentation quality. Segmentation of an image is a process of grouping pixels to form the multiple regions based on different properties of the image such as texture or gray tone [211]. The segmentation of a medical image extracts the regions and contours belong to the different tissues. Previously, many techniques have been proposed for medical image segmentation [212]. In general, the segmentation methods can be classified into thresholding, clustering, region growing and edge detection.

Fuzzy c-mean (FCM) is a clustering based segmentation algorithm, where each data point is assigned to all cluster centers with a membership value, hence contains more information in comparison to hard segmentation. It is one of the most effective method for the classification of MRI data [213]. However, standard FCM [214] is highly sensitive to noise, as it does not consider spatial information. In order to overcome this problem, many studies have been considered local spatial information in the objective function [124, 215]. These segmentation algorithms were parameter dependents, later Stelios Krinidis and Vassilios Chatzis proposed parameter free local information based FCM [216]. The major drawback of FCM based

algorithms is that these are based on iterative process, hence may stick in the sub-optimal solution. To avoid this problem, many metaheuristics based studies have been done while using genetic algorithm [217], particle swarm optimization [218] and hybrid optimization [77]. However, these methods used single objective function and the single criterion sometimes may not produce adequate results. The multiple criterions can improve the robustness, hence the quality of segmentation results [219]. There are few studies have been done in this regard, while considering two cluster qualities. The multi-objective genetic algorithm based FCM clustering minimizes Xie-Beni index and fitness function of FCM to segment the remote sensing images [220, 221], where the user chooses the best dominant solution from the Pareto front. However, the Pareto front surface has many solutions, hence difficult to evaluate the best solution manually. Previously, Pareto fronts have been reduced to the small set of solution using corrected Rand index for a multi-objective clustering [222], whereas another approach has also been explored ensemble of Pareto fronts [223]. Recently, the multi-objective particle swarm optimization based FCM segmentation considered cluster compactness and edge-based measures as two distinct characteristics [79].

The challenging issue in clustering based segmentation is that they are semi-adaptive in nature and user required to define the number of clusters. To overcome this problem, adaptive cluster number based FCM has been studied, which is depends on the cluster quality measures such as Xie-Beni index and partition entropy coefficient of segmentation [224, 225]. The drawback of Partition coefficient and classification entropy is that these techniques show monotonic tendency over the number of clusters [81]. On the other hand, Xie-Beni depends on the membership of cluster fuzziness, where the value of membership exponent affects the cluster fuzziness. Most of the cluster validity indexes work behind the concept of

better separation of clusters. However, better separation always does not produce satisfactory results in real situations. Additionally, the indexes to obtain the optimum number of clusters naturally depend on the segmentation results produced by the methodology. Hence, there is a requirement of a method that can solve this problem with the accuracy.

The proposed algorithm introduces few improvements and capitalizes three criterion based on (i) compactness, (ii) fuzzy hyper-volume, and (iii) classification entropy to produce better segmentation. The proposed algorithm considers local spatial and gray level information in the input. It simultaneously minimizes the cluster compactness and the fuzzy hyper-volume. These two objective functions optimize using an efficient multi-objective antlion optimization (MOALO) [200] based algorithm. The selection of dominant solution from the Pareto fronts is based on minimum partition entropy (PE) coefficient [214]. Further, the present study adaptively calculates the number of clusters present in the image, while considers the cluster volume, cluster compactness, difference between the clusters and minimum number of compact and crispy clusters.

Section 7.2 formulates the local spatial information based FCM with the help of MOALO. Section 7.3 introduces the new index to determine the optimum number of clusters in an image. Section 7.4 discusses material and methods used in the present study. Section 7.5 presents the results of proposed algorithms on simulated images and dataset images. Finally, section 7.6 draws the conclusion of the present study.

7.2 Multi-objective Antlion optimization

Antlion optimization is a nature inspired evolutionary algorithm, which provides superior results in terms of exploitation, exploration and local optima avoidance [98]. The Multi-objective Antlion optimization (MOALO) proposed by S. Mirjalili et al. in 2016 [200], which

simulate the hunting behavior of an antlion. The antlion builds a pit in the shape of the cone, where the edge of the cone is sufficiently sharp to fall an ant at the bottom of it. Antlion waits for the ant underneath the bottom of the cone and tries to catch it there.

Ants move randomly in the search space, and this movement is modeled as follows:

$$S(t) = [0, cums(2r(t_1) - 1), \dots cums(2r(t_n) - 1)] \quad (7.1)$$

where $cums$ evaluates the cumulative sum, t is the number of iteration, n is the maximum number of iterations and $r(t)$ is the random function, which is defined as follows:

$$r(t) = \begin{cases} 1 \; if \; rand > 0.5 \\ 0 \; if \; rand \leq 0.5 \end{cases}$$

The boundaries of the random walk are normalized to restrict the random walks of ants in the search space, which is given as follows:

$$S_i^t = \frac{(s_i^t - a_i) \times (d_i^t - c_i^t)}{(b_i - a_i)} + c_i^t \quad (7.2)$$

where a_i and b_i are the minimum and maximum of the random walks of i^{th} variable respectively, whereas c_i^t and d_i^t are the minimum and maximum of the i^{th} variable in t^{th} iteration respectively.

The trap created by antlion affects the random walks of ants. The following equations model this phenomenon in the following manner:

$$c_i^t = Antlion_j^t + c^t \quad (7.3)$$

$$d_i^t = Antlion_j^t + d^t \quad (7.4)$$

where $Antlion_j^t$ represents the position of the j^{th} antlion, c^t and d^t are the minimum and maximum of all variables in t^{th} iteration respectively. Once ant trapped in the cone, it tries to escape out. The antlion start throw sands to slide down the ant, hence random walks of ant start decreasing in the following manner:

$$c^t = \frac{c^t}{I} \tag{7.5}$$

$$d^t = \frac{d^t}{I} \tag{7.6}$$

where $I = 10^w \frac{t}{n}$, and w is a constant and helps to regulate the accuracy of exploitation. After catching the ant, the selected antlion using roulette wheel reconstruct the cone shaped pit as follows:

$$Antlion_j^t = Ant_j^t, \quad if\ F(Ant_j^t) < F(Antlion_j^t)$$

where Ant_j^t shows the position of ant in t^{th} iteration. Further, the best antlion calculated in every iteration has been kept and known as elite. These elite have the capability to affect the movement of all ants during the iteration. Hence, MOALO considers that all ants randomly move around the elite antlion, similar to movement around a selected antlion. The following equation has been proposed as follows:

$$Ant_j^t = \frac{R_E^t + R_A^t}{2} \tag{7.7}$$

where R_E^t is the random movement around the elite and R_A^t is the random movement around the selected antlion.

7.2.1 Fitness Functions

Ahmed et al. modified standard FCM algorithm by adding the local information to its objective function [226]. Further, Szilagyi et al. pre-calculated the weighted sum image with the help of image obtained by the average of local neighbors and the original image to speed up the process [124]. The first fitness of this algorithm is based on this methodology.

Assume a dataset $X = [x_{11} \dots x_{lp} \dots x_{lm}]$ have c number of clusters. A window of 3×3 is considered around the p^{th} pixel to calculate the local mean. The mean filtered and original intensity levels used to compute the normalized local weighted sum ξ_p of p^{th} pixel as follows:

$$\xi_p = \frac{1}{1+\mu}\left(x_p + \frac{\mu}{N_p}\sum_{r \in N_r} x_r\right) \tag{7.8}$$

where x_r represent the neighbor pixels in the window around x_p, and N_p are the number of neighbor pixels. The parameter μ used to control the neighborhood effect. The pre-calculated data ξ obtained from Equation (7.8) for all pixels in an image. Let the total number of intensity levels in image ξ are q, which is small in comparison to N. The number of pixels have intensity value equal to l denoted by γ_l. Hence, $\sum_l^q \gamma_l = N$. Hence, the objective is defined as follows:

$$J_{\text{EnFCM}} = \sum_{i=1}^{c}\sum_{l=1}^{q} \gamma_l \, u_{il}^m \, (\xi_l - v_i)^2 \tag{7.9}$$

where c is the number of clusters, u_{il} represent the fuzzy membership of l^{th} pixel with respect to i^{th} cluster, m is the exponent and v_i is the center of the cluster. The cluster center and membership function used in Equation (7.9) is defined as follows:

$$u_{il} = \left[\sum_{i=1}^{c} \left(\frac{\xi_l - v_i}{\xi_l - v_i}\right)^{2/m-1}\right]^{-1} \quad (7.10)$$

$$v_i = \frac{\sum_{l=1}^{q} \gamma_l \, u_{il}^m \, \xi_l}{\sum_{l=1}^{q} \gamma_l \, u_{il}^m} \quad (7.11)$$

Fuzzy hyper-volume (FHV) is independent of different sizes, shapes, and cardinality between the clusters [84] and is a good measure of cluster quality in comparison to other [87, 227]. Hence, present study considered FHV as the second fitness function. FHV is defined as follows [228]:

$$FHV = \sum_{i=1}^{c} |\sum_i|^{1/2} \quad (7.12)$$

where $\sum_i$ is the fuzzy covariance matrix, which is defined as follows:

$$\sum_i = \frac{\sum_{l=1}^{q} u_{il}^m (\xi_l - v_i)(\xi_l - v_i)^T}{\sum_{l=1}^{q} u_{il}^m} \quad (7.13)$$

The objective is formulated by aggregating these two fitness functions. This study defines multi-objective optimization problem as:$[minimize \ J_{\text{EnFCM}}(\xi), minimize \ FHV(\xi)], where$ $J_{\text{EnFCM}}(\xi)$ states the compactness of the cluster and $FHV(\xi)$ responsible for clear separation, minimum cluster volume and maximum data concentrated in the neighborhood of the cluster centroid [228]. The first fitness function has been calculated using Equation (7.9), whereas the second fitness function has been calculated using Equation (7.12).

7.2.2 Selection of optimal Pareto front

Multi-objective optimization produces a set of non-dominant solutions. Each of these solutions represents a different segmentation results for a fixed number of clusters. This work selects the optimal solution based on minimum partition entropy (PE) coefficient, and the

minimum of PE produces crisper cluster among the available non-dominant solutions. Hence, the solution corresponds to minimum PE is a dominant solution, which is given as follows:

$$S_{PF} = \min_{s=1:s_n} [PE(u,c)] \tag{7.14}$$

where s are the number of non-dominate solution in the Pareto front surface, PE is defined as follows:

$$PE(u,c) = -\frac{1}{q}\sum_{l=1}^{q}\sum_{i=1}^{c} u_{il}{}^{2}\log(u_{il}) \tag{7.15}$$

Algorithm 7.1 summarizes the working of proposed MOALO based FCM segmentation.

Algorithm 7.1

Requirement: The degree of fuzziness $m = 2$, number of clusters, maximum MOALO iterations and number of ants

Calculate weighted sum image ξ of the input image X

Randomly initialize the ant's population (present study considers clusters' center) with the help of range of pixel values

for** maximum number of iterations **do

for** each ant **do

Select a random antlion from the archive

Select the elite from archive using a roulette- wheel

Modify c and d using equation (7.5) and (7.6) to restrict towards antlion's position

Form random walk and normalize to keep it inside the search-space using equation (7.2)

Update ant's position using equation (7.7)

end for

Compute the objective values, J_{EnFCM} *and* FHV *for all ants according to equation (7.9) and (7.12)*

Update the contents of archive

end for

for *each Pareto fronts* ***do***

Calculate the partition entropy (PE) according to (7.15)

end for

Find the minimum PE and the cluster centers respective to this Pareto front

Updated membership functions according to new clusters' center

Construct the segmented image

7.3 Determination of cluster number

The role of segmentation index is to determine the number of clusters of an image in unsupervised manner. Previously, *Pakhira et al.* measured the cluster quality while considering the small number of compact clusters and obtained significant results on the considered dataset [229]. The adaptive cluster number in the texture segmentation was analyzed using techniques such as mean squared error, partition coefficient, Xie-Beni index

and proposed a combined validity criterion [224]. Further, *Zanaty* analyzed eighteen popular cluster indexes on synthetic images and simulated dataset of MRI images to automatic determine the cluster number and found that the kernelized FCM with spatial constraints combined with AIC obtained the highest accuracy 80% for simulated MRI data [87]. Automatic identification of the number of clusters in unsupervised clustering algorithm is a challenging task, as the most of the cluster performance measures produced unsatisfactory results [86]. Hence, there is a need for an index that can estimate the goodness of cluster with the accuracy.

This study proposes an index called cluster number validity (CNV) index, which combines multiple cluster qualities such as high intra-cluster compactness, higher inter-cluster distance, and minimum cluster volume. Simultaneously, it tries to reduce the number of compact clusters and crispiness of the clusters, which further minimizes the effect of noise and outliers. The proposed index is formulated as follows:

$$CNV = \frac{FHV \times J_{\mathrm{EnFCM}}}{c \times PE \times D^2}$$

where D is the interclass cluster distance, c is the cluster number, FHV defined in (12) and PE defined in (15). The cluster number corresponding to the minimum value of CNV ensures the optimum number of segments in an image. In the numerator, the minimum value of J_{EnFCM} helps to maximize the cluster compactness, at the same time minimum value of FHV helps to minimize the cluster volume. In the denominator, c tries to reduce the number of compact clusters whereas PE helps to decrease the crispiness of clusters and D_{max} increases the distance between the clusters. In the practical situation, if the image is being segmented in more than the actual segments it has, the noise and outliers start to participate in the

segmentation, and hence the role of c and PE in denominator becomes important to fix this problem. Further, the problem of monotonicity at the higher number of clusters observed in FHV compensated by partition entropy coefficient, at the same time knee values reflects in CNV. All these factors lead to CNV index a better segmentation quality index of an image. The CNV index has been tested on 32 synthetic images and 30 simulated MRI dataset of images.

Algorithm 7.2

Calculate weighted sum image ξ of the input image X

for** 2 to c_{max} **do

Consider algorithm 1 as a subroutine

Calculate the SSV of segmented image

end for

Find the segmented image corresponding to minimum SSV

7.4 Material and Methods

The present study includes eight ground truth synthetic images in the size of 256×256 having three, four, five and six number of clusters contains different structures. These images were added with Gaussian (additive in nature) and speckle noise (multiplicative in nature) of different variances to analyze the robustness of the algorithm as given in Table 7-1. In addition to this, the present study has considered dataset of 30 simulated MRI images obtained from BrainWeb (www.bic.mni.mcgill.ca/brainweb/) [230]. The MRI dataset includes T1 weighted simulated MRI images in the size of 181×217 affected by 9% noise, 7% noise with 20% inhomogeneity and 9% noise with 20% inhomogeneity (90th, 92th, 93rd,

94^{th} 95^{th} , 96^{th}, 97^{th}, 98^{th}, 99^{th} and 100^{th} slice). The ground truth images respective to noisy MRI dataset have been used for quantitative analysis of segmentation. MRI dataset images consist of only four segments i.e. gray matter (GM), white matter (WM), cerebral spinal fluid (CSF) and background. The proposed MOALO based FCM segmentation algorithm has been tested on total 54 images (excluding 8 synthetic ground truth images) whereas proposed CNV cluster validity index has been tested and validated on total 62 images.

Table 7-1: Details of noisy synthetic images used in the study

S. No.	Total Images	Number of clusters	Noise Variance (Gaussian)	Noise Variance (Speckle)
1.	6	3	0.1, 0.05	0.05
2.	6	4	0.05, 0.03	0.025
3.	6	5	0.05, 0.03	0.025
4.	6	6	0.02, 0.01	0.02

7.4.1 Segmentation quality measurements

The segmentation quality of proposed MOALO based FCM algorithm and other methods used for comparison calculated by optimal segmentation accuracy (SA) [225], Jaccard similarity (JS) and Dice coefficient (DC) [231]. All these segmentation measures evaluate the similarity between the images in different ways, which given as follows: $SA(X,Y) = \frac{|I_i \cap G_i|}{|G_i|}$, $JS(I_i,\ G_i) = \frac{|I_i \cap G_i|}{|I_i \cup G_i|}$ and $DC(I_i,\ G_i) = \frac{2|I_i \cap G_i|}{|I_i|+|G_i|}$, where I_i and G_i represent the pixels belongs to i^{th} segment of segmented image and ground truth image respectively. The higher values of these indexes denote the better segmentation performance. The maximum output value of

these measures can be one, which means the two images are the same. This study shows these measurements in percentage.

7.5 Results and discussion

The present study first demonstrates the noise robustness capability of the algorithm. The proposed MOALO based FCM algorithm has been compared with classical Fuzzy c-mean proposed by *Bezdek* [214], modified FCM with spatial constraints FCM_S1, FCM_S2 [215], enhanced FCM [124], and texture primitive feature based FCM (FCM_TPF) [187]. Further, this study validates the CNV index that determines the optimal number of clusters in an image. The proposed index has been compared with other popular cluster quality indexes such as Xie-Bei, FHV and PE indexes.

Figure 7.1 shows the segmentation results for the image having five number of clusters and affected by Gaussian noise (variance =0.05), whereas Fig. 7.2 shows segmentation results for the image having six number of clusters and affected by speckle noise (variance=0.02). Visually, it can be observed that the segmentation results obtained by classical FCM are highly affected by noise. The FCM_S1, FCM_S2 and Enhanced FCM (EnFCM, α=1.2) resist to noise more in comparison to classical FCM but unsatisfactory especially in such high noise. The FCM_TPF algorithm works better in the case of the image having greater noise, however, yields poor results in the case of six number of clusters as results shown in Fig. 7.2. The segmentation results show that the proposed algorithm outperforms FCM, FCM_S1, FCM_S2 EnFCM and FCM_TPF in the presence of high noise and the higher number of clusters. Table 7-2 shows the quantitative evaluation of results, where the segmentation accuracy of the images has been calculated in terms of JS, DC and SA. The average result for all considered synthetic images in presence of noise shows that the proposed algorithm works

better than the other segmentation algorithms. It shows motivating results especially, where all other algorithm fails to deliver in case of images have noise and the higher number of clusters.

The algorithm has been tested on simulated MRI dataset in the presence of noise and intensity inhomogeneity. Figure 7.3 shows the qualitative comparison of proposed algorithm with other considered FCM based algorithm. The segmentation results in the figure show that proposed algorithm produces satisfactory results for the 90th slice of MRI image corrupted by 9% noise. Table 7-3 shows mean segmentation accuracy of thirty MRI images and reveal that the proposed algorithm outperforms FCM, FCM_S1, FCM_S2 EnFCM and FCM_TPF at different noise levels and inhomogeneity. Please note, up to this level of study the number of clusters in the input image was known and kept same.

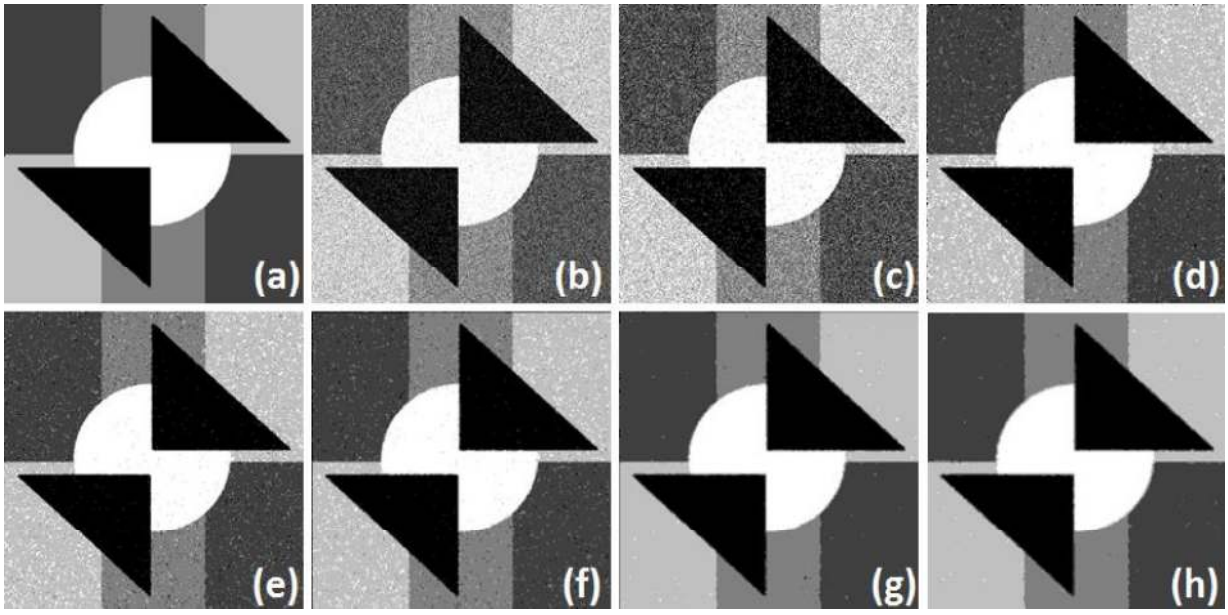

Figure 7-1: Segmentation results for synthetic image having five clusters and corrupted by Gaussian noise (0.05 variance), (a) ground truth image, (b) input image, segmented images obtained using (c) FCM, (d) FCM_S1, (e) FCM_S2, (f) EnFCM, (g) FCM_TPF and (f) proposed algorithm

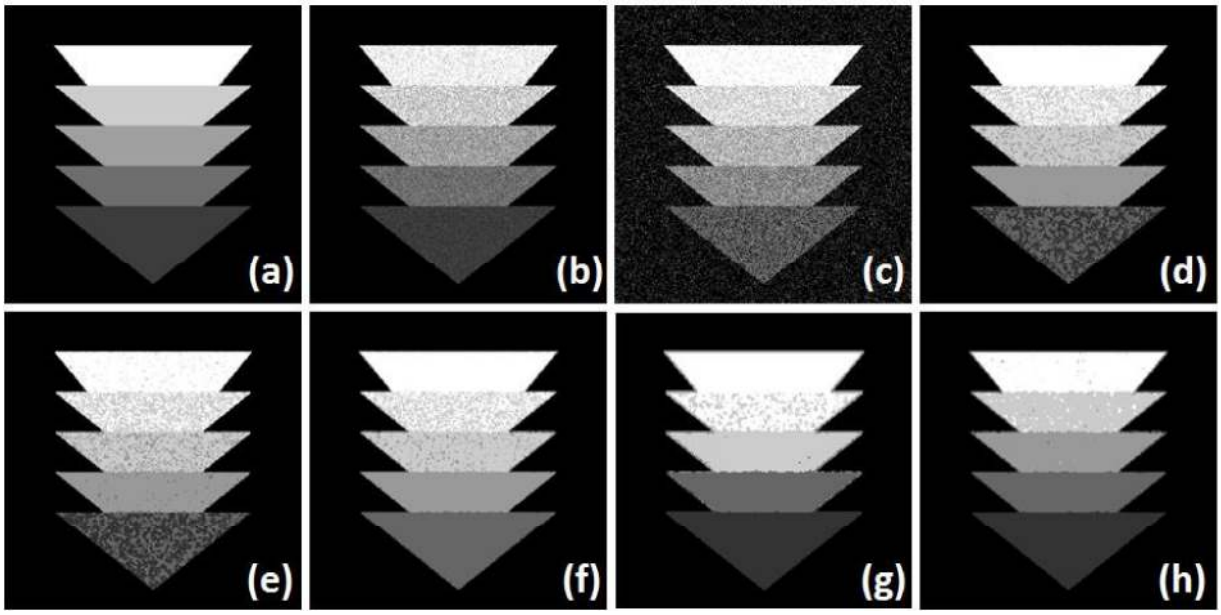

Figure 7-2: Segmentation results for synthetic image having six clusters and corrupted by Speckle noise (0.02 variance), (a) ground truth image, (b) input image, segmented images obtained using (c) FCM, (d) FCM_S1, (e) FCM_S2, (f) EnFCM, (g) FCM_TPF and (f) proposed algorithm

Table 7-2: Segmentation accuracy of twenty-four synthetic images suffered from Gaussian and speckle noise

Clusters	Evaluation Criterion	Segmentation methods					
		FCM	FCM_S1	FCM_S2	EnFCM	FCM_TPF	Proposed Method
3	JS	85.754	94.183	84.899	96.008	98.949	99.110
	DC	91.626	96.761	88.631	97.790	99.464	99.544
	SA	92.537	96.792	89.782	97.803	99.493	99.542
4	JS	75.208	95.548	95.116	97.483	99.137	99.148
	DC	84.202	97.679	97.436	98.706	99.565	99.570
	SA	87.484	98.123	97.909	99.013	99.579	99.542
5	JS	60.654	86.089	80.622	90.602	97.328	97.293
	DC	73.155	92.099	87.574	94.801	98.637	98.615
	SA	76.940	93.899	90.433	96.366	98.742	98.974

	JS	47.448	38.829	54.815	58.811	48.910	95.889
6	DC	60.587	48.826	64.337	65.782	55.386	97.882
	SA	63.522	51.529	66.327	71.346	57.611	97.918
	JS	67.266	78.662	78.863	85.726	86.081	97.860
Average	DC	77.392	83.842	84.494	89.270	88.263	98.903
	SA	80.120	85.086	86.113	91.132	88.856	98.994

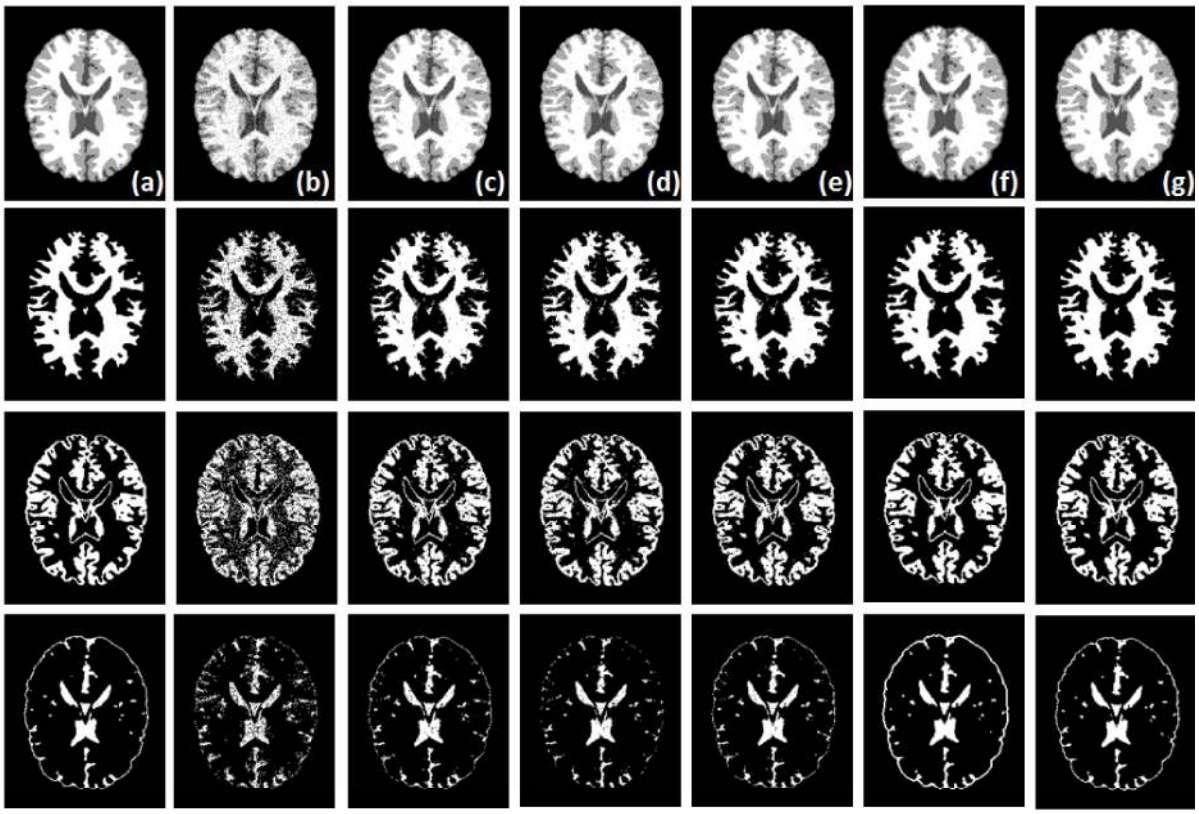

Figure 7-3: Segmentation results for 90th slice simulated MRI image corrupted by 9% noise. (a) First column images from up to below shows segmented ground truth image, its WM, GM and CSF respectively. (b) Second column images shows segmentation results for noisy input image, WM, GM and CSF obtained using FCM, (c) FCM_S1, (d) FCM_S2, (e) EnFCM, (f) FCM_TPF and (g) proposed algorithm

Table 7-3: Mean segmentation accuracy (with standard deviation) for thirty MRI dataset images (including ten 9% noise with 0% inhomogeneity, ten 9% noise with 20% inhomogeneity and ten 7% noise with 20% inhomogeneity)

Method	Evaluation Criterion	Mean of thirty MRI dataset images			Average
		WM	GM	CSF	
FCM	JS	81.80±4.53	66.93±8.51	64.26±11.27	71.00±11.48
	DC	89.92±2.72	79.88±6.29	77.67±8.73	82.49±8.30
	SA	86.57±5.22	81.54±6.49	83.49±3.37	83.87±5.53
FCM_S1	JS	91.09±1.21	82.28±2.34	82.16±4.42	85.18±5.13
	DC	95.34±0.66	90.26±1.41	90.14±2.69	91.91±3.01
	SA	94.62±0.90	90.10±1.60	93.35±1.91	92.69±2.44
FCM_S2	JS	90.91±1.26	83.36±2.28	82.42±4.96	85.57±4.98
	DC	95.24±0.69	90.91±1.35	90.28±3.03	92.14±2.94
	SA	94.78±0.92	90.36±1.55	94.59±1.28	93.24±2.41
EnFCM	JS	92.11±0.94	84.21±1.84	84.49±3.20	86.94±4.28
	DC	95.89±0.51	91.42±1.09	91.56±1.89	92.96±2.45
	SA	95.31±0.86	91.28±1.21	94.36±1.74	93.65±2.17
FCM_TPF	JS	89.53±1.23	82.94±1.92	88.41±2.74	86.96±3.54
	DC	94.47±0.69	90.66±1.15	93.77±1.50	92.97±2.02
	SA	99.00±0.62	87.21±1.95	89.99±2.69	92.07±5.42
Proposed method	JS	93.72±0.89	88.28±1.30	89.35±1.92	90.45±2.77
	DC	96.75±0.48	93.77±0.74	94.37±1.08	94.96±1.53
	SA	96.14±0.87	94.15±0.70	95.09±0.64	95.13±1.11

Further, this study validates the proposed CNV index to determine the number of clusters in an image. The CNV index has been calculated while keeping the number of clusters variable for proposed MOALO based FCM. The maximum range of the number of clusters has been

kept to seven, as it has been observed that MOALO based FCM can correctly find the six segment in a ground truth image. Figure 7.4 shows that proposed CNV index produces satisfactory results for images having the different number of clusters corrupted by different noise and noise levels. Xie-Beni, PE, and FHV indexes have been calculated for the segmented images also obtained from proposed MOALO based FCM algorithm for the comparative analysis. Figure 7.4 (a) is an example of the noisy image that has three clusters, where Xie-Beni could not reach to the minimum value at 3 cluster number and PE index shows monotonicity over the number of clusters. On the other hand, FHV and proposed CNV index correctly determined the number of clusters, as obtained minimum value at 3 clusters. Figure 7.4 (b) is an example of ground truth image has four clusters, where all indexes correctly obtain the number of clusters except PE index. Proposed CNV index performs well for images having five and six clusters with Gaussian and speckle noise respectively as shown in Fig. 7.4 (c, d). Figure 7.4 (e) shows the goodness of proposed CNV index, where Xie-Beni, FHV and PE all failed to determine the correct number of clusters for the synthetic MRI image. Table 7-4 shows the overall accuracy of proposed index on the synthetic dataset of thirty-two images and MRI dataset of thirty images. The table reveals that the proposed CNV index outperforms other in its class.

The proposed MOALO based FCM optimally segments the image, which is based on the criterions: compactness, FHV and partition entropy. Hence, the accuracy of CNV index also depends on the segmentation quality of proposed MOALO based FCM. Further, to generalize this index intensive experiment with other FCM based algorithm is required.

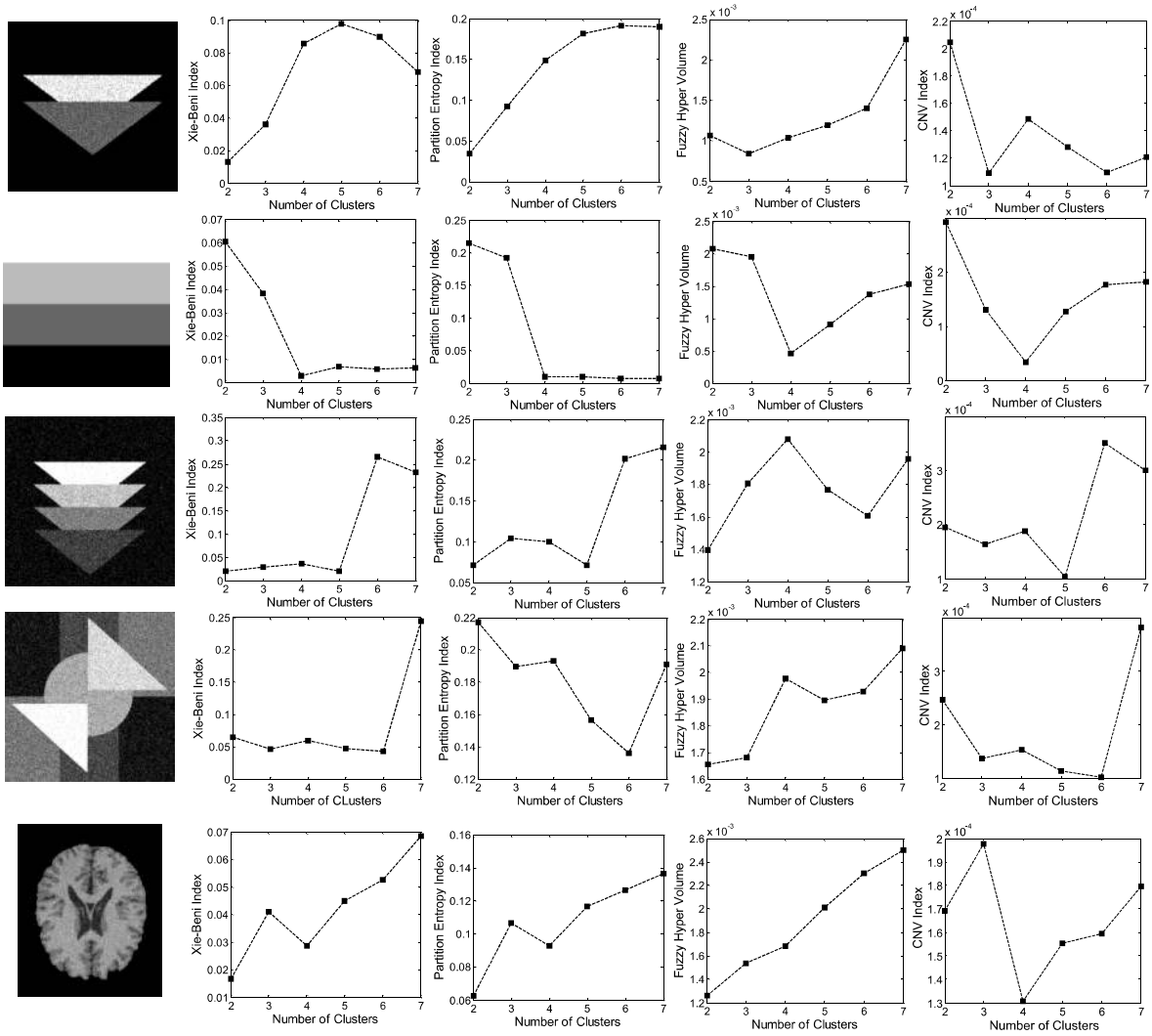

Figure 7-4: Comparison of proposed CNV index with Xie-Beni, Partition entropy coefficient and Fuzzy Hyper Volume for different cases. (a) Synthetic image has three clusters and suffered from speckle noise (0.05 variance), (b) synthetic image have four clusters without noise, (c) synthetic image has five clusters and suffered from Gaussian noise (0.03 variance) (d) synthetic image has five clusters and suffered from speckle noise (0.02 variance), (e) 92nd slice of simulated MRI image has four clusters and corrupted by 9% noise with 20% inhomogeneity

Table 7-4: Comparison of validity indexes for detection of correct number of clusters

Image Type	No. of Images	Number of Correct Classification			
		XB	PE	FHV	Proposed
Synthetic image with 6 clusters	8	6	8	2	7
Synthetic image with 5 clusters	8	7	8	7	8
Synthetic image with 4 clusters	8	7	7	6	8
Synthetic image with 3 clusters	8	3	4	6	7
Simulated MRI with 9% noise	10	0	0	0	5
Simulated MRI with 7% noise, 20% inhomogeneity	10	0	0	0	8
Simulated MRI with 9% noise 20% inhomogeneity	10	0	0	0	9
Overall Success rate		37.09%	43.45%	33.87%	83.87%

7.6 Conclusions

The present study demonstrated two significant contributions: (i) proposed multi-objective optimization using MOALO based FCM algorithm improves the robustness to the noise, and hence the segmentation quality and (ii) proposed an efficient cluster validity index. These proposed algorithms have been tested and validated on a large dataset of synthetic images and simulated MRI images. The synthetic images consist of a few objects synthesized by assigning certain values to the group of pixels, whereas simulated MRI images were downloaded from BrainWeb, this study uses these set of images as the gold standard. The comparison of proposed MOALO based FCM with other considered FCM algorithms has been performed, where the proposed algorithm has shown its effectiveness with highest mean accuracy 97.86%, 98.90%, 98.99% respectively in terms of JS, DC, SA on synthetic images, whereas 90.45%, 94.96%, 95.13% respectively in terms of JS, DC, SA on simulated MRI images. The proposed cluster number validity index, CNV attains minimum value when the

image has the appropriate number of clusters. This index has been extensively compared with Xie-Beni, FHV and PE indexes, where it has delivered comparatively better performance with the highest accuracy of 83.87%.